# Polyethylenimine as a dual functional additive for electron transporting layer in efficient solution processed planar heterojunction perovskite solar cells†

Sujuan Dong,[ab] Yangyang Wan,[ab] Yaling Wang,[ab] Yin Yang,[ab] Yahui Wang,[ab] Xinyu Zhang,[ab] Huanqi Cao,[ab] Wenjing Qin,[ab] Liying Yang,*[ab] Cong Yao,*[c] Ziyi Ge*[d] and Shougen Yin*[ab]

We report a doping method to enhance the performance of solution processed planar heterojunction perovskite solar cells. By doping a small percentage (3 wt%) of polyethylenimine (PEI) as additive into the PCBM electron transport layer of an inverted perovskite solar cell, which led to significant enhancements of power conversion efficiency from (5.9 ± 0.2) % to (10.4 ± 0.2) %. The AFM images show that the PEI doped PCBM layer can help to form a high quality, homogeneous and compact electron transporting layer on the rough $CH_3NH_3PbI_3$ layer, which results in enhanced hole blocking ability and reduced leakage current at the interfaces between the $CH_3NH_3PbI_3$, PCBM films and the top Al electrode. Organic field-effect transistors (OFETs) measurements reveal that the addition of 1–3 wt% PEI into PCBM layer can improve device performance without any negative effect on the electron transport property of PCBM. Steady-state PL analysis shows that the electron-rich PEI may also act as an effective interfacial modifier to passivate the trap states at the perovskite surface or crystal boundaries and to avoid the undesired charge recombination often observed in perovskite solar cells. PEI will also improve performance as a cathode interfacial modifier because the PCE of the device with PEI deposited between PCBM and Al is superior to the device without PEI. This work demonstrated that amine-containing polymer materials can be used as an efficient dual functional additive in perovskite solar cells. This study provides an efficient way of developing highly efficient $CH_3NH_3PbI_3$-based perovskite solar cells.

## Introduction

The organic–inorganic hybrid perovskite solar cells have shown great potential as one of the most promising candidates for low-cost solar energy conversion over the past decade.[1–4] This kind of perovskite absorbers have received a great deal of attention because of their superior properties such as direct band gap, broad light absorption, long exciton diffusion lengths (100–1000 nm), bipolar transport and high carrier mobility.[5] The power conversion efficiency (PCE) of perovskite solar cells has been demonstrated with an unbelievable speed increased from 3.8% to 21.1% in the last few years.[6] Further PCE enhancements can be realized by preventing recombination *via* interface engineering and improving the quality of the perovskite film. The conventional device structure (FTO/compact $TiO_2$/mesoporous $TiO_2$/perovskite/hole transporting material/anode) has been widely used. However, the fabrication of mesoporous $TiO_2$ layer needs a high-temperature (over 400 degrees) sintering process which will result in higher cost and slower production. Therefore, as an alternative approach, the inverted planar heterojunction perovskite solar cells with a structure of ITO/PEDOT:PSS/perovskite/electron transporting layer/cathode only requires cost-efficient low temperature fabrication process emerges in response to the needs of time.[7–10] The planar architecture is attractive in developing large-area, flexible perovskite and multi-junction (or tandem) construction. The perovskite layer is inserted between a hole-transport layer (PEDOT:PSS) and an electron transporting layer (PCBM). One of the crucial problems lies in the choice of electron transporting layer for inverted perovskite solar cells is so limited. Fullerene and its derivatives with high electron mobility and efficient

[a]*Key Laboratory of Display Materials and Photoelectric Devices, Education Ministry of China, School of Materials Science and Engineering, Tianjin University of Technology, Tianjin 300384, China. E-mail: liyingyang@tjut.edu.cn; sgyin@tjut.edu.cn*

[b]*Tianjin Key Laboratory for Photoelectric Materials and Devices, Tianjin University of Technology, Tianjin 300384, China*

[c]*China Electronics Technology Group Corporation No. 18th Research Institute, Tianjin 300384, China. E-mail: huobingyao@vip.qq.com*

[d]*Ningbo Institute of Materials Technology & Engineering, Chinese Academy of Sciences, Ningbo 315201, China. E-mail: geziyi@nimte.ac.cn*

electron injection property have been exclusively used. However, it is questionable to be the final choice for future large scale production of large-area solution processed perovskite solar cells due to its high cost and poor ambient stability. Furthermore, although there have been many efforts to improve the processing technology of the perovskite film in inverted planar heterojunction structure,[8,9] yet, it is still a great challenge to obtain a high quality, uniform and pin-hole free perovskite layer through a solution spin-coating process. Therefore, the subsequent PCBM layer deposited on the rough perovskite surface generally shows poor film-forming performance. Interfacial engineering is a powerful strategy to enhance efficiency and stability of perovskite solar cells. Li and co-workers employed TIPD as an electron transporting layer to form an ohmic contact with the negative electrode, aiming to enhance the charge extraction and suppress the charge recombination.[10] Bai and co-workers fabricated a planar structure perovskite solar cell by adding a small percentage (~1.5 wt%) of polystyrene (PS) into the PCBM solution. It is found that the addition of PS as a film-forming additive improves the electron transporting layer uniformity and decreases the recombination.[11] However, the PS is an insulating polymer and it has not any passivation effect on the trap states at the perovskite surface and crystal boundaries, which have been regarded to be detrimental to charge transporting.[12,13] The existence of trap states leads to undesired charge recombination in the perovskite layer and may be a reason for the phenomena of hysteresis.[14–16] Noel *et al.* regards the vacancy of halide to be the origin of the surface defects. The loss of $I^-$ will leave the Pb atoms un-coordinated which may become the centre for recombination of carriers and induce a low current density and fill factor (FF).[13] A convenient and efficient way to passivate surface defects is to treat the perovskite film with electron-rich molecules. The electron-rich materials will provide excess electrons to neutralize the positive ions of perovskite, thereby passivate surface defects. Polyethylenimine (PEI) and its polyethylenimine ethoxylated (PEIE) has been reported as an efficient interfacial layer to decrease work function of cathode[17] and used for interfacial engineering in the field of organic solar cells and perovskite solar cell.[18–21] The nitrogen atom of the amine-containing side of PEI is also an electron rich functional group. It may provide electrons to the Pb atoms and form a coordinate or dative-covalent bond with the perovskite surface, thus passivate the surface defects. In this paper, we use PEI as a doping additive in PCBM layer and successfully fabricate efficient planar perovskite solar cells in ambient conditions.

# Experimental

## Materials

PEI (average $M_w \sim 25\,000$ by LS) was obtained from Aldrich Co. Fullerene derivative (PCBM) with purity over 99% was obtained from Solenne B.V., Netherlands. $PbI_2$ (99.999%) was purchased from Aldrich Co. An aqueous dispersion of PEDOT:PSS (Baytron® P VP AI 4083) was obtained from Heraeus Co. All the materials were used as received. $CH_3NH_3I$ was synthesized using the same method as published in the literature.[22] ITO-coated glass with a sheet resistance of 10 Ω per square is used for device fabrication. The routine cleaning procedure includes ultra-sonication in a solution of detergent, deionized water, and isopropyl alcohol in sequence.

## Device fabrication and performance measurements

$PbI_2$ of 231 mg $ml^{-1}$ in *N*,*N*-dimethylformamide (DMF) was stirred at 70 °C for 3 h, $CH_3NH_3I$ of 38 mg $ml^{-1}$ in isopropanol (IPA) was stirred at room temperature for 3 h, PCBM of 24 mg $ml^{-1}$ in *o*-dichlorobenzene was stirred at 70 °C for 12 h. PEI dissolved in ethanol with a concentrations of 6 mg $ml^{-1}$ was added to the PCBM solution from 1 to 5 wt% in the ratio of PCBM.

Fig. 1 shows the structure of the devices and the energy level diagram of the respective device components. The preparation procedure of the device is described as follows. The PEDOT:PSS layer of about 40 nm was obtained by spin-coating at 3000 rpm for 30 s on ITO coated glass substrates, followed by drying at 120 °C for 30 minutes on hotplate in air. The $CH_3NH_3PbI_3$ layer was deposited by two-step spin-coating method. First, a layer of $PbI_2$ was spin-coated on top of the PEDOT:PSS with a spin-rate of 6000 rpm for 30 s. After the $PbI_2$ film was dried at 70 °C for 10 minutes in air, $CH_3NH_3I$ solution was loaded on the $PbI_2$ film for 20 s (loading time), which was spun at 6000 rpm for 20 s and then annealed at 60 °C for 10 minutes followed by 100 °C for 20 minutes. Then 40 nm PCBM film doped with or without PEI was deposited by spin-coating (through controlling the speed and calibrated with a surface profiler) on top of $CH_3NH_3PbI_3$ layer. PEI was deposited between PCBM and Al at 6000 rpm for 30 s for the reference devices with a structure of ITO/PEDOT:PSS/$CH_3NH_3PbI_3$/PCBM/PEI/Al. Finally, 120 nm Al layer was thermally evaporated under a vacuum of a pressure of $1 \times 10^{-4}$ Pa. All the fabrication and characterization procedures were performed in an ambient atmosphere at room temperature. The thickness for $CH_3NH_3PbI_3$, PCBM or PEI doped PCBM layer is about 260 nm and 40 nm, respectively. The active layer area of the device is 0.09 $cm^2$ defined by a shadow mask.

The current density–voltage (*J*–*V*) characteristics of the unencapsulated devices were measured under intensity of 100 mW $cm^{-2}$ illuminations by using a 300 W solar simulator with an AM1.5G filter. The light intensity was calibrated with an Oriel mono-Si reference cell (CROWNTECH PVM 272 certificated by NREL). The absorption spectrum was measured by UV-4100 UV-vis spectrophotometer. The surface roughness and morphology

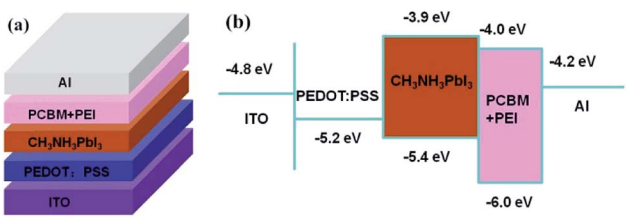


Fig. 1 (a) Device structure of the planar heterojunction perovskite solar cell; (b) schematic energy level diagram of the device.

of the $PbI_2$, $CH_3NH_3PbI_3$, $CH_3NH_3PbI_3$/PCBM and $CH_3NH_3PbI_3$/PCBM + (1–5 wt%) PEI layers were characterized by Bruker INNOVA SPM in tapping mode. The thickness of the above layers was measured by a surface profiler (KLA Tencor Alpha Step D-100). Steady-state PL was recorded with a Jobin Yvon FluoroLog-3 fluorescence spectrometer.

## Results and discussion

### Device performance

Fig. 2 shows the *J–V* curves of the best perovskite solar cell with 3 wt% PEI additive and without PEI additive measured in forward bias. The *J–V* curves of the best perovskite solar cell with 3 wt% PEI additive were measured in forward and reverse bias with a scan speed of 500 mV $s^{-1}$ (Fig. 3). The $J_{SC}$ obtained by integration of the incident photon-to-electron conversion efficiency (IPCE) spectra agrees well with the $J_{SC}$ obtained from the *J–V* measurement in Fig. 3(b). The detailed device performance parameters including short-circuit current density ($J_{SC}$), FF, open-circuit voltage ($V_{OC}$) and PCE are summarized in Table 1. *J–V* curves of the best devices with different PEI doping concentration are shown in Fig. S1 (ESI†). The reference device with pristine PCBM as ETL only achieved a PCE value of (5.9 ± 0.2) %, with $V_{OC}$ of (0.81 ± 0.01) V, $J_{SC}$ of (14.34 ± 1.13) mA $cm^{-2}$ and FF of (50.9 ± 0.9) %. As showed in Fig. 2 and Table 1, for the device with the addition of PEI to PCBM, the best efficiency is obtained when PEI doping concentration is 3 wt%. The addition of 3 wt% PEI increases the $V_{OC}$ from (0.81 ± 0.01) to (0.96 ± 0.02) V, the $J_{SC}$ from (14.34 ± 1.13) mA $cm^{-2}$ to (15.54 ± 0.35) mA $cm^{-2}$ and the FF from (50.9 ± 0.9) % to (68.9 ± 0.7) %, and led to a PCE of (10.4 ± 0.2) %, which represents a significant enhancement in PCEs over the pristine PCBM-based device. This efficiency improvement can be attributed to the simultaneous increase of the $V_{OC}$, FF and $J_{SC}$.

Fig. S2 (ESI†) shows the *J–V* curve of the best device with a structure of ITO/PEDOT:PSS/$CH_3NH_3PbI_3$/PCBM/PEI/Al. The detailed device performance parameters are summarized in Table S1 (ESI†) together with the control device. Compared with the control device, the PCE increased from 6.1% to 7.0%, with the $V_{OC}$ increased from 0.81 V to 0.84 V, $J_{SC}$ increased from 14.51 mA $cm^{-2}$ to 14.96 mA $cm^{-2}$, and FF from 52.3% to 55.7%. The improvement of the performance with PEI deposited between PCBM and Al indicates that PEI will also modify the cathode

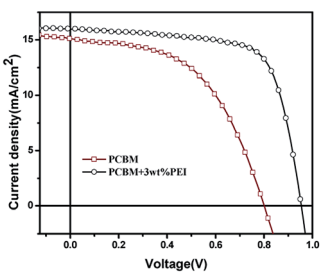


Fig. 2 The current density–voltage (*J–V*) curves of devices for the best device with 3 wt% PEI doping concentration and without doping.

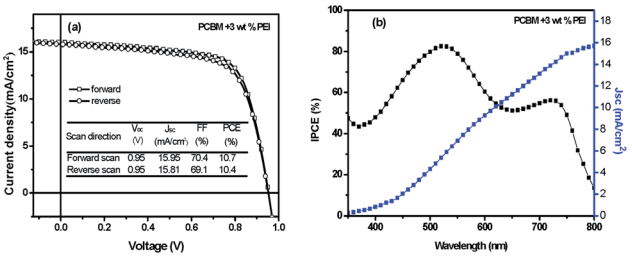


Fig. 3 (a) The current density–voltage (*J–V*) characteristics and (b) external quantum efficiency curve of devices for the best device with 3 wt% PEI doping concentration.

interface to improve the performance when used as an additive in PCBM.

To investigate the electron transport ability of the pristine PCBM and PEI doped PCBM, we fabricated organic field-effect transistors (OFETs) in the bottom-gate, top-contact configuration using PCBM and PEI doping PCBM as channel materials. All devices employed heavily doped n-type Si substrate as the gate electrode, 300 nm thick $SiO_2$ as the insulating layer. Finally, 150 nm Al layer was thermally evaporated under vacuum defined by a shadow mask to obtain the source electrode and the drain electrode. The transfer characteristics of representative devices ($V_{DS}$ was fixed at 50 V) are shown in Fig. S3 (ESI†). In the saturation region, the drain to source current ($I_{DS}$) is determined by eqn (1). Eqn (2) used to calculate carrier mobility can be deduced from eqn (1).

$$I_{DS} = \frac{W}{2L} C_i \mu (V_{GS} - V_T)^2 \quad (1)$$

$$\mu = \frac{2L}{WC_i} \left( \frac{\partial {I_{DS}}^{1/2}}{\partial V_{GS}} \right)^2 \quad (2)$$

In the above equations, $V_T$ is the threshold voltage, obtained from the transfer characteristics curve; $C_i$ is the capacitance/unit area of the oxide layer (8.6 nF $cm^{-2}$); $W$ and $L$ are the channel width (50 μm) and channel length (5000 μm), respectively. We can obtain the value of electron mobility by the slope of ${I_{DS}}^{1/2}$–$V_{GS}$ according to eqn (1).

The electron mobility of all measured films is shown in Table 2. The pristine PCBM film has an electron mobility of (6.5 ± 0.3) × $10^{-4}$ $cm^2$ $V^{-1}$ $s^{-1}$. The electron mobility of PCBM film doped with 1–3 wt% PEI is (7.3 ± 0.2) × $10^{-4}$ $cm^2$ $V^{-1}$ $s^{-1}$, (7.9 ± 0.3) × $10^{-4}$ $cm^2$ $V^{-1}$ $s^{-1}$, (6.8 ± 0.5) × $10^{-4}$ $cm^2$ $V^{-1}$ $s^{-1}$ respectively. The enhanced electron mobility of 1 wt% and 2 wt% PEI doping in PCBM film may be attributed to the dipole formed at the interface between the molecular PEI and PCBM which facilitates the electron transporting. Doping 3 wt% PEI in PCBM has merely higher electron mobility than pure PCBM, but lower than the sample of 1 wt% and 2 wt% PEI doping concentration. This result is reasonable because PEI is a kind of insulating polymer. Even so, the addition of 1–3 wt% of PEI seems to improve device performance without any negative effect on the electron transport property of the PCBM layer. In

Table 1 Summary of the device performance for the perovskite solar cells with different PEI doping concentration

| Doping concentration of PEI | | $V_{OC}$ (V) | $J_{SC}$ (mA cm$^{-2}$) | FF (%) | PCE (%) |
|---|---|---|---|---|---|
| Pure PCBM | Average | (0.81 ± 0.01) | (14.34 ± 1.13) | (50.9 ± 0.9) | (5.9 ± 0.2) |
| | Best | 0.81 | 14.51 | 52.3 | 6.1 |
| PCBM + 1 wt% PEI | Average | (0.87 ± 0.01) | (14.76 ± 0.54) | (55.8 ± 1.2) | (7.3 ± 0.3) |
| | Best | 0.88 | 15.27 | 56.5 | 7.6 |
| PCBM + 2 wt% PEI | Average | (0.92 ± 0.02) | (14.99 ± 0.37) | (58.3 ± 2.2) | (8.0 ± 0.3) |
| | Best | 0.90 | 15.52 | 58.2 | 8.1 |
| PCBM + 3 wt% PEI | Average | (0.96 ± 0.02) | (15.54 ± 0.35) | (68.9 ± 0.7) | (10.4 ± 0.2) |
| | Best | 0.95 | 15.95 | 70.4 | 10.7 |
| PCBM + 4 wt% PEI | Average | (0.88 ± 0.02) | (13.46 ± 0.66) | (59.1 ± 1.9) | (7.0 ± 0.4) |
| | Best | 0.89 | 13.95 | 59.4 | 7.4 |
| PCBM + 5 wt% PEI | Average | (0.87 ± 0.01) | (10.85 ± 0.78) | (56.8 ± 1.2) | (5.3 ± 0.4) |
| | Best | 0.86 | 11.65 | 58.8 | 5.9 |

addition, it has been proved that PEI can lower the work function of Al cathode[17] and reduce the contact resistance and facilitate a better ohmic contact formation at the cathode interface. The improved cathode interface results in better devices performance with higher $V_{OC}$. However, excessive amount of PEI additive (4 wt% and 5 wt%) would detrimentally affect the electron transport ability of the PCBM layer and thus reduce the device performance parameters including $V_{OC}$ and $J_{SC}$. As a result, the 4 wt% and 5 wt% PEI doped PCBM films show much lower electron mobility of $(3.8 \pm 0.2) \times 10^{-4}$ cm$^2$ V$^{-1}$ s$^{-1}$, $(1.5 \pm 0.2) \times 10^{-4}$ cm$^2$ V$^{-1}$ s$^{-1}$, respectively.

### Atomic force microscopy

To gain deep insights into the PEI doped PCBM layer, we also take atomic force microscopy (AFM) measurements of the film of perovskite ($CH_3NH_3PbI_3$), PCBM and PEI doped PCBM to investigate the morphological change of these films. The surface morphology of the two-step spin-coating method prepared perovskite films is typically very rough due to tendency for crystallization (SEM images in ESI Fig. S4†). In our conditions, the $R_q$ roughness of a 260 nm thick perovskite layer is ~16 nm, with peak to valley height larger than 120 nm (ESI Fig. S5†). Therefore, a relatively thick PCBM layer (>40 nm) is required to form a conformal coating on the perovskite surface to reduce of current shorting through pinholes. Fig. 4 shows 5 μm × 5 μm images of the AFM topography, phase image and section analysis of the PCBM films (without or with 3 wt% PEI) coated on perovskite layer. The root mean square roughness ($R_q$), mean roughness ($R_a$) and peak to valley distance estimated from the AFM images show the differences of the two samples. It can be seen that the spin-coated film of PCBM doped with 3 wt% PEI exhibits a much smoother surface than the pure PCBM film. The $R_q$ and $R_a$ for the pristine PCBM film are 11.0 and 7.91 nm, respectively. Because the PCBM solution is a low viscosity and thus it is difficult to form a compact surface. The rough surface may lead to a poor interface between PCBM and Al electrode, thus cause a large leakage current. This may be the reason for the low performance of the control device. The addition of PEI increases the viscosity of PCBM solution. As a result, it becomes much easier to form a high quality, homogeneous and compact PCBM electron transporting layer. The $R_q$ and $R_a$ value for the 3 wt% PEI doped PCBM film decrease to 4.47 and 3.28 nm,

Table 2 Summary of the electron mobility of PCBM doped with different PEI concentration

| Films | Electron mobility $\mu_e$ ($\times 10^{-4}$ cm$^2$ V$^{-1}$ S$^{-1}$) |
|---|---|
| Pristine PCBM | 6.5 ± 0.3 |
| PCBM + 1 wt%PEI | 7.3 ± 0.2 |
| PCBM + 2 wt%PEI | 7.9 ± 0.3 |
| PCBM + 3 wt%PEI | 6.8 ± 0.5 |
| PCBM + 4 wt%PEI | 3.8 ± 0.2 |
| PCBM + 5 wt%PEI | 1.5 ± 0.2 |

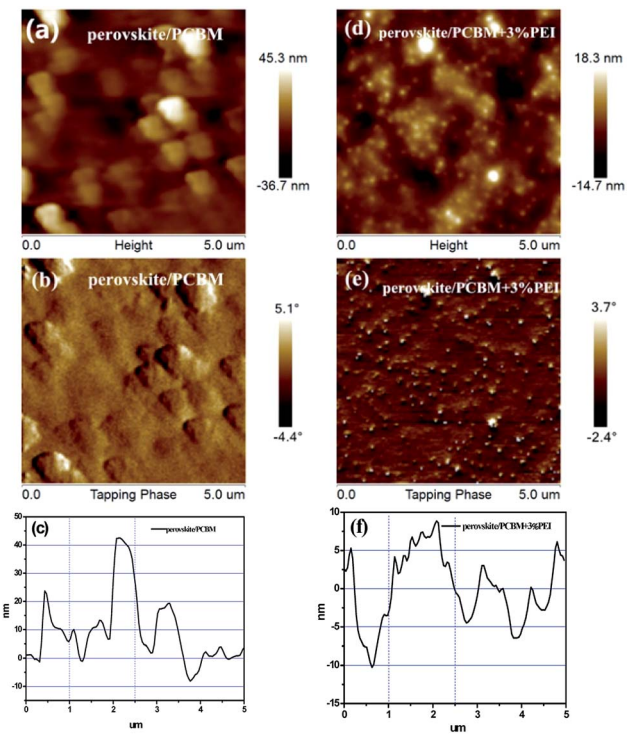


Fig. 4 The AFM topography, phase image and section analysis of the PCBM films (without or with 3 wt% PEI) coated on the perovskite layer.

respectively. The increase of $V_{OC}$ value from 0.81 V to 0.95 V can be explained by the better coverage of PEI doped PCBM layers, which results in enhanced hole blocking ability and reduced current leakage at the interfaces between the perovskite, PCBM film and the top Al electrode. However, excessive addition of the insulating PEI causes irregular formation of PEI aggregates (Fig. S5 in ESI†). This may be the reason for the decreased $V_{OC}$ and FF when doping concentration is 4 wt% and 5 wt%. The 5 μm × 5 μm AFM images of the PEI deposit onto the PCBM layer are shown in Fig. S6.† The roughness of the film ($R_q$ = 13.9 nm, $R_a$ = 10.0 nm) is similar to that of PCBM film. So, it can't improve the film uniformity by simply coating PEI on PCBM film.

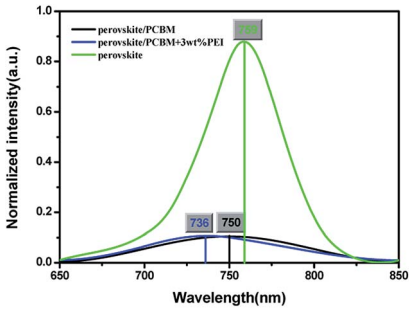


Fig. 5 Steady-state PL spectra of the perovskite, perovskite/PCBM, perovskite/PCBM + 3 wt% PEI films.

### UV-vis absorption spectra and photoluminescence (PL) analysis

The absorption for perovskite/PCBM film and perovskite/PCBM + (1–5 wt%) PEI film was measured (Fig. S7 in ESI†). The absorption spectra of the PCBM films (without or with PEI doping) coated on perovskite layer are nearly identical. So the addition of PEI into PCBM solution doesn't have any negative influence on the absorbance property.

Recently, the presence of trap states at the surfaces and grain boundaries of perovskite crystals was considered to be one of the reasons that result in undesired charge recombination in the perovskite layer, which leads to the large photocurrent hysteresis. Therefore, it is critically important to develop effective methods to passivate the trap states to further promote the performance of the perovskite solar cells. It has been reported that the presence of trap states could induce band bending close to the surface of the perovskite film, which led to an apparent band gap lower than that of the bulk with a red-shifted PL peak. Filling the trap states enables the recovery of the band gap and blue-shifts the PL peak.[12] So, steady-state PL is a simple and effective way to investigate the presence of the defects state. Hence, we measured the steady-state PL of perovskite, perovskite/PCBM and perovskite/PCBM doped with PEI to study the trap filling effect between the perovskite/PCBM interfaces. The samples we prepared only have an interface, namely, the interface between perovskite and PCBM (or PCBM + PEI), so we can measure the interface between perovskite and ETL no matter which side the incident excitation light is from. Here, the incident excitation light was from the air side (not the glass side). As showed in Fig. 5, the PL peak of pristine perovskite without a PCBM layer is located at 759 nm, which is smaller than previously reported.[12] As expected, the PL intensity of perovskite/PCBM or perovskite/PCBM + PEI is strongly lowered than pristine $CH_3NH_3PbI_3$ film, indicates PCBM and PCBM + PEI are good PL quenchers for the perovskite films. Fig. 5 shows that the PL peak of perovskite/PCBM is shifted from 759 nm to 750 nm, suggests PCBM can decrease the surface defects close to the top surface and/or along the grain boundaries of perovskite film, which is observed in the previous report.[8] The perovskite/PCBM + 1–5 wt% PEI films show a PL peak at 746 nm, 740 nm, 736 nm, 745 nm and 753 nm, respectively (Fig. S8†). Although all the three samples showed similar decline in PL intensity, the PL peaks of the perovskite films were obviously different. Perovskite film coated with the PCBM + 3 wt% PEI showed an apparent blue-shifted PL peak from 759 nm to 736 nm, which demonstrates that surface trap states decrease. Therefore, we postulate that one of the plausible reasons for the significant improvement of device performance when PCBM + 3 wt% PEI was used as the ETL is attributing to the effective trap states passivation at the perovskite/PCBM interface.

## Conclusions

In summary, a small percentage (3 wt%) of PEI as additive is added into the PCBM electron transport layer of an inverted perovskite solar cell, which led to significant enhancements of PCE from (5.9 ± 0.2) % to (10.4 ± 0.2) %. The AFM images show that the PEI doped PCBM layer can help to form a high quality, homogeneous and compact electron transporting layer covered on the perovskite layer, which results in enhanced hole blocking ability and reduced leakage current at the interfaces between the perovskite, PCBM films and the top Al electrode. OFETs measurements revealed the addition of 3 wt% of PEI into PCBM seems to improve device performance without any negative effect on the electron transport property of PCBM. Meanwhile, steady-state PL analysis shows that the electron-rich PEI may also act as an effective interfacial modifier to passivate the trap states at the perovskite surface or crystal boundaries. So that, avoid the undesired charge recombination often observed in $CH_3NH_3PbI_3$-based perovskite solar cells. At last, PEI will also play as a cathode interfacial modifier to improve the performance by facilitating an ohmic contact with Al cathode. This work demonstrates that amine-containing polymer materials can be used as an efficient dual functional additive for electron transporting layer in perovskite solar cells, and we believe that this study can provide a simple and effective approach to further promote the performance of $CH_3NH_3PbI_3$-based perovskite solar cells after extended investigation.

## Acknowledgements

The authors are grateful to the Tianjin Natural Science Council (Grant No. 13JCYBJC18900, 13JCZDJC26700), National High Technology Research and Development Program of China (863

Program) (Grant No. 2013AA014201), National Key Scientific Instrument and Equipment Development Project (2014YQ120351) and the Tianjin Key Discipline of Material Physics and Chemistry for the support of this work.

## Notes and references


1 A. Kojima, K. Teshima, Y. Shirai and T. Miyasaka, *J. Am. Chem. Soc.*, 2009, **131**, 6050–6051.

2 N. J. Jeon, J. H. Noh, W. S. Yang, Y. C. Kim, S. Ryu, J. Seo and S. Il Seok, *Nature*, 2015, **517**, 476–480.

3 W. S. Yang, J. H. Noh, N. J. Jeon, Y. C. Kim, S. Ryu, J. Seo and S. Il Seok, *Science*, 2015, **348**, 1234–1237.

4 M. A. Green, A. H. Baillie and H. J. Snaith, *Nat. Photonics*, 2014, **8**, 506–514.

5 A. Mei, X. Li, L. Liu, Z. Ku, T. Liu, Y. Rong, M. Xu, M. Hu, J. Chen, Y. Yang, M. Grätzel and H. Han, *Science*, 2014, **345**, 295–298.

6 M. Saliba, T. Matsui, J. Seo, K. Domanski, J. Correa-Baena, M. K. Nazeeruddin, S. M. Zakeeruddin, W. Tress, A. Abate, A. Hagfeldtd and M. Grätzel, *Energy Environ. Sci.*, 2016, **9**, 1989–1997.

7 J. You, Z. Hong, Y. Yang, Q. Chen, M. Cai, T. Song, C. Chen, S. Lu, Y. Liu, H. Zhou and Y. Yang, *ACS Nano*, 2014, **8**, 1674–1680.

8 Q. Guo, C. Li, W. Qiao, S. Ma, F. Wang, B. Zhang, L. Hu, S. Dai and Z. Tan, *Energy Environ. Sci.*, 2016, **9**, 1486–1494.

9 C. Li, Q. Guo, W. Qiao, Q. Chen, S. Ma, X. Pan, F. Wang, J. Yao, C. Zhang, M. Xiao, S. Dai and Z. Tan, *Org. Electron.*, 2016, **33**, 194–200.

10 C. Li, F. Wang, J. Xu, J. Yao, B. Zhang, C. Zhang, M. Xiao, S. Dai, Y. Li and Z. Tan, *Nanoscale*, 2015, **7**, 9771–9778.

11 Y. Bai, H. Yu, Z. Zhu, K. Jiang, T. Zhang, N. Zhao, S. Yang and H. Yan, *J. Mater. Chem. A*, 2015, **3**, 9098–9102.

12 Y. Shao, Z. Xiao, C. Bi, Y. Yuan and J. Huang, *Nat. Commun.*, 2014, **5**, 5784.

13 N. K. Noel, A. Abate, S. D. Stranks, E. S. Parrott, V. M. Burlakov, A. Goriely and H. J. Snaith, *ACS Nano*, 2014, **8**, 9815–9821.

14 A. Abate, M. Saliba, D. J. Hollman, S. D. Stranks, K. Wojciechowski, R. Avolio, G. Grancini, A. Petrozza and H. J. Snaith, *Nano Lett.*, 2014, **14**, 3247–3254.

15 D. Shi, V. Adinolfi, R. Comin, M. Yuan, E. Alarousu, A. Buin, Y. Chen, S. Hoogland, A. Rothenberger, K. Katsiev, Y. Losovyj, X. Zhang, P. A. Dowben, O. F. Mohammed, E. H. Sargent and O. M. Bakr, *Science*, 2015, **347**, 519–522.

16 F. Gao, Z. Li, J. Wang, A. Rao, I. A. Howard, A. Abrusci, S. Massip, C. R. McNeill and N. C. Greenham, *ACS Nano*, 2014, **8**, 3213–3221.

17 Y. Zhou, C. F. Hernandez, J. Shim, J. Meyer, A. J. Giordano, H. Li, P. Winget, T. Papadopoulos, H. Cheun, J. Kim, M. Fenoll, A. Dindar, W. Haske, E. Najafabadi, T. M. Khan, H. Sojoudi, S. Barlow, S. Graham, J. Brédas, S. R. Marder, A. Kahn and B. Kippelen, *Science*, 2012, **336**, 327–332.

18 S. Woo, W. H. Kim, H. Kim, Y. Yi, H. Lyu and Y. Kim, *Adv. Energy Mater.*, 2014, **4**, 1301692.

19 L. Yan, Y. Song, Y. Zhou, B. Song and Y. Li, *Org. Electron.*, 2015, **17**, 94–101.

20 H. Zhang, H. Azimi, Y. Hou, T. Ameri, T. Przybilla, E. Spiecker, M. Kraft, U. Scherf and C. J. Brabec, *Chem. Mater.*, 2014, **26**, 5190–5193.

21 H. Zhou, Q. Chen, G. Li, S. Luo, T. Song, H. Duan, Z. Hong, J. You, Y. Liu and Y. Yang, *Science*, 2014, **345**, 542–546.

22 L. Etgar, P. Gao, Z. Xue, Q. Peng, A. K. Chandiran, B. Liu, M. K. Nazeeruddin and M. Grätzel, *J. Am. Chem. Soc.*, 2012, **134**, 17396–17399.